Letters

Frequency-Selective Suppression Method of Harmonic Magnetic Field for Double-Sided *LCC* Wireless Power Transfer Systems

Seongho Woo, *Student Member, IEEE*, Yujun Shin, *Member, IEEE*, Jaewon Rhee, Hyunsoo Lee, *Student Member, IEEE*, Hongseok Kim, *Member, IEEE*, and Seungyoung Ahn, *Senior Member, IEEE*

***Abstract*—This letter proposes a method for selectively reducing harmonic magnetic field. When a wireless power transfer (WPT) system transmits power using a magnetic field as a medium, a leakage magnetic field inevitably occurs nearby. Meanwhile, a square wave voltage is generated by high-frequency switching of the inverter or rectifier used in the WPT system, and this square wave voltage is divided into fundamental and harmonic components. Harmonic components are radiated through the coil and can cause interference in other electronic devices, resulting in an electromagnetic interference (EMI) problem. The proposed method selectively and completely reduces harmonics by modifying the double-sided *LCC* topology. The approach was verified through an experiment, showing that the third harmonic and fifth harmonic can be reduced by 16.03 and 18.27 dB, respectively.**

***Index Terms*—Double-sided *LCC* topology, electromagnetic interference (EMI), wireless power transfer (WPT) system.**

I. Introduction

WIRELESS power transfer (WPT) technology has been employed in various applications that require low power as well as high power [1], [2], [3]. This versatility is achieved by using a magnetic field as the medium to wirelessly transfer power from the transmitter (TX) to the receiver (RX). During the transfer process, a leakage magnetic field inevitably occurs. This leakage magnetic field can cause a malfunction or even damage to other electronic devices, a problem known as electromagnetic interference (EMI) in WPT systems.

Previously, to mitigate harmonic radiated fields, a reactive shielding method and adding a series inductor were proposed. In [4], a method of shielding two components was proposed, but because it adds a coil, it had the disadvantages of increasing the volume of the system. Hong et al. [5] proposed an optimal resonant frequency for the shield coil to selectively shield EMI. However, because it was applied to a tightly coupled WPT system for mobile applications, it did not consider EMI generated in the RX. Sim et al. [6] proposed a shield coil design method that reduces EMI while increasing efficiency. The reported performance was 1.1 dB, which is insufficient, and the location of the shielding coil was in the exact center of the TX and RX coils, making it unsuitable for actual applications. Shin et al. [7] proposed an EMI suppression method that added a series inductor in a series–series (SS) topology. In the SS topology, adding more series inductors improves EMI performance. However, as the inductance increases, the parasitic resistance also increases, which can lead to a significant decrease in power transfer efficiency.

This letter proposes a method to selectively and completely cancel harmonics in the double-sided *LCC* topology, which is widely used in WPT systems. Section II explains the principle of selectively cancelling harmonics. In Section III, the proposed method is verified through experiment. Finally, Section IV concludes this letter.

II. Method for Selectively Suppressing a Harmonic Magnetic Field

Fig. 1 shows the EMI source of the WPT system. Typically, WPT systems use an inverter and a rectifier, which are composed of switching elements such as MOSFETs and diodes. As a result, these power electronics circuits generate a square wave voltage. This square wave voltage contains harmonic components, and WPT systems generally exhibit odd harmonic components, which are the primary cause of EMI issues [8].

Fig. 2 shows the proposed double-sided *LCC* topology. The resonance condition of the existing double-sided topology can

Received 20 September 2024; revised 26 October 2024; accepted 24 November 2024. Date of publication 27 November 2024; date of current version 28 January 2025. This work was supported in part by the Institute of Information and Communications Technology Planning and Evaluation under Grant RS-2024-00399304 (Development of Lightweight Materials and Electromagnetic Field Reduction Technology for Wireless Power Transfer System for 22 kW Electric Vehicles, 60%) and Grant 2020-0-00839 (Development of Advanced Power and Signal EMC Technologies for Hyperconnected E-Vehicle, 40%) funded by the Korea Government (Ministry of Science and ICT), and in part by ANSYS Korea. *(Corresponding author: Seungyoung Ahn.)*

Seongho Woo, Jaewon Rhee, Hyunsoo Lee, and Seungyoung Ahn are with the CCS Graduate School of Mobility, Korea Advanced Institute of Science and Technology, Daejeon 34051, South Korea (e-mail: seongho@kaist.ac.kr; elly0386@kaist.ac.kr; hyunsoolee@kaist.ac.kr; sahn@kaist.ac.kr).

Yujun Shin is with the Department of Automotive Engineering, Keimyung University, Daegu 42601, South Korea (e-mail: yjshin@kmu.ac.kr).

Hongseok Kim is with the CCS Graduate School of Mobility, Korea Advanced Institute of Science and Technology, Daejeon 34051, South Korea, and also with CPS Tech, Inc., Seoul 08590, South Korea (e-mail: kimhongseok@kaist.ac.kr).

Color versions of one or more figures in this article are available at https://doi.org/10.1109/TPEL.2024.3507874.

Digital Object Identifier 10.1109/TPEL.2024.3507874

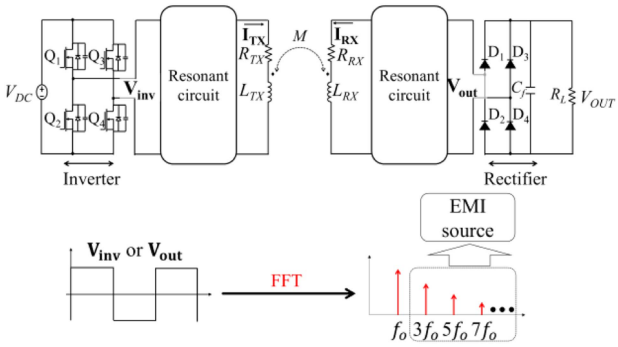

Fig. 1. EMI sources of the WPT system due to the power electronic circuits.

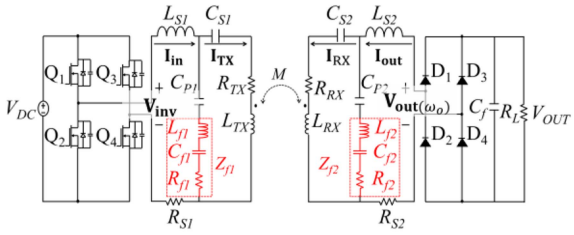

Fig. 2. Proposed double-sided *LCC* topology in a WPT system to selectively suppress EMI.

be summarized as follows [9]:

$$\omega_o = \frac{1}{\sqrt{L_{S1}C_{P1}}} = \frac{1}{\sqrt{(L_{\mathrm{TX}} - L_{S1})C_{S1}}} = \frac{1}{\sqrt{L_{S2}C_{P2}}} = \frac{1}{\sqrt{(L_{\mathrm{RX}} - L_{S2})C_{S2}}}. \tag{1}$$

Fig. 3 shows the equivalent circuit of the double-sided *LCC* topology depending on the frequencies. Fig. 3(a) shows the equivalent circuit of the double-sided *LCC* topology at the operating frequency. Equation (2), represents the general form of the Kirchhoff's voltage law (KVL) equations for the four loops in Fig. 2, including both the fundamental and harmonic components, and is expressed in a matrix form (2) shown at the bottom of this page, where

$$Z^n{}_{11} = jn\omega_o L_{s1} + \frac{1}{jn\omega_o C_{p1}}$$

$$Z^n{}_{22} = \frac{1}{jn\omega_o C_{p1}} + \frac{1}{jn\omega_o C_{s1}} + jn\omega_o L_{TX}$$

$$Z^n{}_{33} = \frac{1}{jn\omega_o C_{p2}} + \frac{1}{jn\omega_o C_{s2}} + jn\omega_o L_{RX}$$

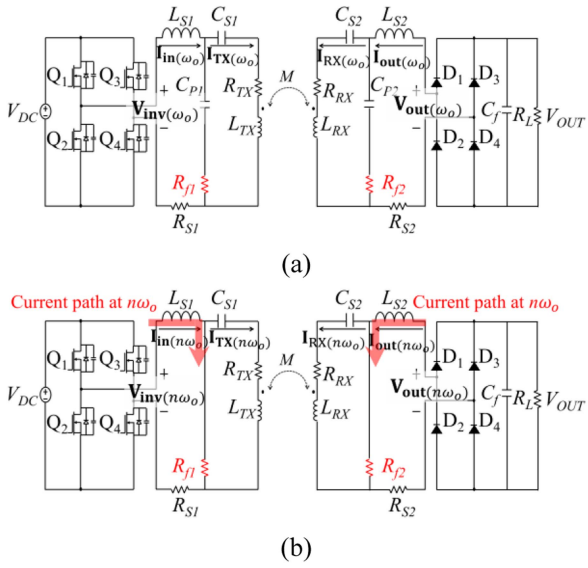

Fig. 3. Double-sided *LCC* topology depending on the frequencies (a) at the operating frequency and (b) at the harmonic frequencies.

$$Z^n{}_{44} = jn\omega_o L_{s2} + \frac{1}{jn\omega_o C_{p2}}$$

$$Z^n{}_{12} = Z^n{}_{21} = -\frac{1}{jn\omega_o C_{p1}}$$

$$Z^n{}_{34} = Z^n{}_{43} = -\frac{1}{jn\omega_o C_{p2}}$$

$$f(L_{f1}) = jn\omega_o L_{f1} + \frac{1}{jn\omega_o C_{f1}}$$

$$f(L_{f2}) = jn\omega_o L_{f2} + \frac{1}{jn\omega_o C_{f2}}$$

$$(n = 1, 3, 5, \ldots). \tag{3}$$

The matrix equation in (2), when n equals 1, represents the KVL at the operating frequency. When (4) is satisfied, $\mathbf{I_{in(\omega_o)}}$, $\mathbf{I_{TX(\omega_o)}}$, $\mathbf{I_{RX(\omega_o)}}$, and $\mathbf{I_{out(\omega_o)}}$ can be expressed as in (5)

$$\omega_o = \frac{1}{\sqrt{L_{f1}C_{f1}}} = \frac{1}{\sqrt{L_{f2}C_{f2}}} \tag{4}$$

$$\mathbf{I_{in(\omega_o)}} = jC_{P1}C_{P2}M{\omega_o}^3\mathbf{V_{out(\omega_o)}}$$

$$\mathbf{I_{TX(\omega_o)}} = -j\omega_o C_{P1}\mathbf{V_{inv(\omega_o)}}$$

$$\mathbf{I_{RX(\omega_o)}} = -j\omega_o C_{P2}\mathbf{V_{out(\omega_o)}}$$

$$\mathbf{I_{out(\omega_o)}} = jC_{P1}C_{P2}M{\omega_o}^3\mathbf{V_{inv(\omega_o)}} \tag{5}$$

$$\begin{bmatrix} Z^n{}_{11} + f(L_{f1}) & Z^n{}_{12} - f(L_{f1}) & 0 & 0 \\ Z^n{}_{21} - f(L_{f1}) & Z^n{}_{22} + f(L_{f1}) & jn\omega_o M & 0 \\ 0 & jn\omega_o M & Z^n{}_{33} + f(L_{f2}) & Z^n{}_{34} - f(L_{f2}) \\ 0 & 0 & Z^n{}_{43} - f(L_{f2}) & Z^n{}_{44} + f(L_{f2}) \end{bmatrix} \begin{bmatrix} \mathbf{I_{in}} \\ \mathbf{I_{TX}} \\ \mathbf{I_{RX}} \\ \mathbf{I_{out}} \end{bmatrix} = \begin{bmatrix} \mathbf{V_{inv}} \\ 0 \\ 0 \\ \mathbf{V_{out}} \end{bmatrix} \tag{2}$$

where the subscript (ω_o) represents the components of operating frequency.

As shown in (5), the proposed topology retains the characteristic of the double-sided *LCC* topology, where $\mathbf{I_{TX}}_{(\omega_o)}$ and $\mathbf{I_{out}}_{(\omega_o)}$ remain constant regardless of the load.

At the *n*th harmonic frequencies, the harmonic current of $\mathbf{I_{TX}}$ and $\mathbf{I_{RX}}$ should be zero to make the harmonic magnetic field ideally zero. In Fig. 2, the harmonic impedance that contains C_{P1}, L_{f1}, and C_{f1} can be calculated as

$$Z_{p1(n\omega_o)} = \frac{1}{jn\omega_o C_{p1}} + jn\omega_o L_{f1} + \frac{1}{jn\omega_o C_{f1}} + R_{f1} \tag{6}$$

where $Z_{p1(n\omega_o)}$ is the impedance at the *n*th harmonic, which includes C_{P1}, L_{f1}, and C_{f1}.

C_{p1} and C_{f1} can be calculated from (1) and (4) as

$$C_{p1} = \frac{1}{{\omega_o}^2 L_{S1}} \tag{7a}$$

$$C_{f1} = \frac{1}{{\omega_o}^2 L_{f1}}. \tag{7b}$$

Substituting (7) into (6), we obtain

$$\begin{aligned} Z_{p1(n\omega_o)} &= \frac{\omega_o L_{S1}}{jn} + jn\omega_o L_{f1} + \frac{\omega_o L_{f1}}{jn} + R_{f1} \\ &= -j\omega_o \frac{L_{S1} + \left(1-n^2\right) L_{f1}}{n} + R_{f1}. \end{aligned} \tag{8}$$

L_{f1}, which makes an imaginary part of (8) zero, can be calculated as

$$L_{f1} = \frac{L_{S1}}{n^2 - 1}. \tag{9}$$

In addition, if the same condition applies to the RX side, L_{f2} can be calculated as

$$L_{f2} = \frac{L_{S2}}{n^2 - 1}. \tag{10}$$

Fig. 3(b) shows the equivalent circuit of the double-sided *LCC* topology at the harmonic frequencies. The matrix equation in (2) represents the KVL at the harmonic frequencies. When (9) and (10) are satisfied, $\mathbf{I_{in}}_{(n\omega_o)}$, $\mathbf{I_{TX}}_{(n\omega_o)}$, $\mathbf{I_{RX}}_{(n\omega_o)}$, and $\mathbf{I_{out}}_{(n\omega_o)}$ can be expressed as

$$\begin{aligned} \mathbf{I_{in}}_{(n\omega_o)} &= -\frac{j\mathbf{V_{inv}}_{(n\omega_o)}}{L_{S1} n\omega_o} \\ \mathbf{I_{TX}}_{(n\omega_o)} &= 0 \\ \mathbf{I_{RX}}_{(n\omega_o)} &= 0 \\ \mathbf{I_{out}}_{(n\omega_o)} &= -\frac{j\mathbf{V_{out}}_{(n\omega_o)}}{L_{S2} n\omega_o} \end{aligned} \tag{11}$$

where the subscript $(n\omega_o)$ represents the components of the harmonic frequencies.

As shown in (11), when the proposed method is applied, the *n*th current of the TX and RX coils is ideally zero, which means that the harmonic magnetic field is also ideally zero. In practice, due to parasitic resistance and the fact that the resonance of the circuit components in (4), (7), and (9) is not perfectly satisfied, it is impossible to ideally eliminate the harmonic current of the TX and RX coils.

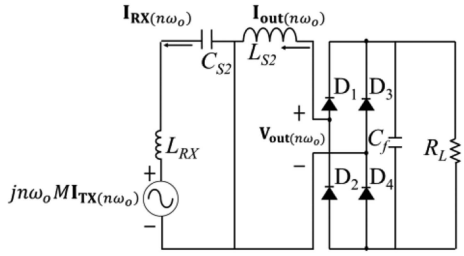

Fig. 4. Equivalent circuit of the RX side at the harmonic frequencies.

There are two sources for the harmonic currents of the TX or RX coils. The first is the harmonic current in the RX coil caused by the harmonic voltage induced in the RX coil by the harmonic current flowing into the TX coil, and the second is the harmonic current in the RX coil caused by the input voltage of the rectifier in the form of a square wave, as shown in Fig. 4. On the RX side, the first source can be eliminated by making the TX harmonic current zero using (9), and the second source can be eliminated by making the harmonic current of the RX coil zero using (10), thus ideally removing all radiated EMI sources. The same applies to the TX side as well.

By applying KVL in Fig. 4, (12) can be obtained, and by calculating $\mathbf{I_{RX}}_{(n\omega_o)}$ and $\mathbf{I_{out}}_{(n\omega_o)}$, (11) can be obtained again

$$\begin{aligned} &jn\omega_o M\ \mathbf{I_{TX}}_{(n\omega_o)} = 0 \\ &= \left(jn\omega_o L_{RX} + \frac{1}{jn\omega_o C_{S2}}\right) \mathbf{I_{RX}}_{(n\omega_o)} \\ &\quad - \mathbf{V_{out}}_{(n\omega_o)} + jn\omega_o L_{S2}\ \mathbf{I_{out}}_{(n\omega_o)} = 0. \end{aligned} \tag{12}$$

In the first KVL in (12), since the induced voltage of the harmonic component from the TX coil is zero, it can be confirmed that $\mathbf{I_{RX}}_{(n\omega_o)}$ is also zero. In the second KVL in (12), because the components C_{P2}, L_{f2}, and C_{f2} act as a short circuit, it can be confirmed that the current caused by $\mathbf{V_{out}}_{(n\omega_o)}$ does not flow through the loop that includes the RX coil.

While the proposed method selectively reduces harmonic components to zero ideally, further analysis of the impact of other harmonics on the system is also necessary. Considering only the TX side in Fig. 2, the conventional system, where L_{f1} and C_{f1} are absent, can be expressed in matrix form using KVL, as shown in (13). Using (1) and (7a), the *n*th harmonic of $\mathbf{I_{TX}}$ is given by (14)

$$\begin{bmatrix} jn\omega_o L_{S1} + \frac{1}{jn\omega_o C_{P1}} & -\frac{1}{jn\omega_o C_{P1}} \\ -\frac{1}{jn\omega_o C_{P1}} & \frac{1}{jn\omega_o C_{P1}} + \frac{1}{jn\omega_o C_{S1}} + jn\omega_o L_{TX} \end{bmatrix} \times \begin{bmatrix} \mathbf{I_{in,conv}} \\ \mathbf{I_{TX,conv}} \end{bmatrix} = \begin{bmatrix} \mathbf{V_{inv}} \\ 0 \end{bmatrix} \tag{13}$$

$$\mathbf{I_{TX}}_{(n\omega_o),\text{conv}} = \frac{n\mathbf{V_{inv}}_{(n\omega_o)}}{-j\omega_o(n^2-1)^2 L_{TX} + j\omega_o L_{S1}}. \tag{14}$$

In addition, considering only the TX side in Fig. 2, the proposed system, where L_{f1} and C_{f1} are present, can be expressed

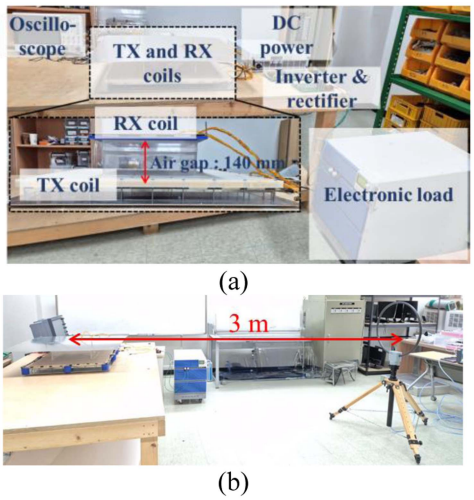

Fig. 5. Experimental setup. (a) Overall system configurations. (b) EMI measurement setup.

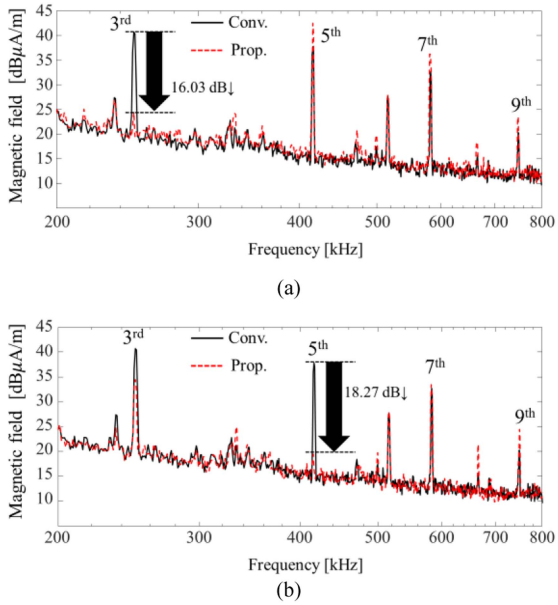

Fig. 6. EMI measurement results when the proposed method is applied (a) for $n = 3$ and (b) for $n = 5$, as indicated in (9) and (10).

in matrix form using KVL, as shown in (15) shown at the bottom of this page. Using (1) and (7b), the nth harmonic of $\mathbf{I_{TX}}$ is given by (16) shown at the bottom of this page,

Depending on the system, specific harmonics can cause EMI issues. For example, if the third harmonic is problematic, using the proposed method, L_{f1} in (9) for $n = 3$ ideally reduces the third harmonic in (16) to zero. When L_{f1} is set to the value for $n = 3$ in (9), the magnitude relations of the third, fifth, seventh, and ninth harmonics for both conventional and proposed systems can be summarized as follows:

$$\begin{aligned}
&\left|\mathbf{I_{TX}}_{(3\omega_o),\text{conv}}\right| > \left|\mathbf{I_{TX}}_{(3\omega_o),\text{prop}}\right| (=0)\\
&\left|\mathbf{I_{TX}}_{(5\omega_o),\text{conv}}\right| < \left|\mathbf{I_{TX}}_{(5\omega_o),\text{prop}}\right|\\
&\left|\mathbf{I_{TX}}_{(7\omega_o),\text{conv}}\right| < \left|\mathbf{I_{TX}}_{(7\omega_o),\text{prop}}\right|\\
&\left|\mathbf{I_{TX}}_{(9\omega_o),\text{conv}}\right| < \left|\mathbf{I_{TX}}_{(9\omega_o),\text{prop}}\right|. \qquad (17)
\end{aligned}$$

Another case occurs when L_{f1} is set to the value for $n = 4$ in (9); the magnitude relations of the third, fifth, seventh, and ninth harmonics for both conventional and proposed systems can be summarized as follows:

$$\begin{aligned}
&\left|\mathbf{I_{TX}}_{(3\omega_o),\text{conv}}\right| > \left|\mathbf{I_{TX}}_{(3\omega_o),\text{prop}}\right|\\
&\left|\mathbf{I_{TX}}_{(5\omega_o),\text{conv}}\right| > \left|\mathbf{I_{TX}}_{(5\omega_o),\text{prop}}\right|\\
&\left|\mathbf{I_{TX}}_{(7\omega_o),\text{conv}}\right| < \left|\mathbf{I_{TX}}_{(7\omega_o),\text{prop}}\right|\\
&\left|\mathbf{I_{TX}}_{(9\omega_o),\text{conv}}\right| < \left|\mathbf{I_{TX}}_{(9\omega_o),\text{prop}}\right|. \qquad (18)
\end{aligned}$$

Therefore, the magnitude of harmonics can vary depending on the value of n. As confirmed in (17), when $n = 3$, the proposed system can ideally reduce the third harmonic to zero, but other harmonics increase. As shown in (18), when $n = 4$, the proposed system cannot ideally eliminate the third and fifth harmonics, but it can reduce them compared to the conventional system, while the seventh and ninth harmonics may increase. From these results, it is evident that reducing a specific harmonic can result in an increase in other harmonics. This suggests that, depending on which specific harmonic poses an issue with respect to the EMI regulations for WPT systems, the value of n in (9) can be selectively adjusted. For example, if the EMI results of a WPT system show that the fifth harmonic significantly exceeds the EMI regulatory limit while other harmonics remain well below the limits, the value of n can be chosen as 5 to address this specific harmonic. On the other hand, if both the third and fifth harmonics slightly exceed the regulatory limits, n can be selected as 4 to balance the reduction of these harmonics. While the proposed method has the clear advantage of being able to completely eliminate a specific harmonic, the tradeoff of increasing other harmonics presents a limitation, and this aspect requires further research.

III. Verification Through Experiment

Fig. 5 shows the experimental setup. As shown in Fig. 5(a), the experiment was conducted with a dc power supply, TX and RX coils, inverter and rectifier, oscilloscope, and electronic load. The output power was set to 500 W in the experiment. Fig. 5(b)

$$\begin{bmatrix} jn\omega_o L_{S1} + \frac{1}{jn\omega_o C_{P1}} + f(L_{f1}) & -\frac{1}{jn\omega_o C_{P1}} - f(L_{f1}) \\ -\frac{1}{jn\omega_o C_{P1}} - f(L_{f1}) & \frac{1}{jn\omega_o C_{P1}} + \frac{1}{jn\omega_o C_{S1}} + jn\omega_o L_{TX} f(L_{f1}) \end{bmatrix} \begin{bmatrix} \mathbf{I_{in,prop}} \\ \mathbf{I_{TX,prop}} \end{bmatrix} = \begin{bmatrix} \mathbf{V_{inv}} \\ 0 \end{bmatrix} \qquad (15)$$

$$\mathbf{I_{TX}}_{(n\omega_o),\text{prop}} = \frac{n\mathbf{V_{inv}}_{(n\omega_o)}\left(\left(n^2-1\right)L_{f1}+L_{S1}\right)}{j\omega_o(n^2-1)^2 L_{TX}\left(L_{f1}+L_{S1}\right)+j\omega_o\left(\left(n^4-1\right)\right)L_{f1}-L_{S1})L_{S1}}. \qquad (16)$$

TABLE I
PARAMETERS OF THE EXPERIMENT

Parameters	Value
Operating frequency	85 kHz
R_L	16 Ω
L_{TX}/R_{TX}	38.5 μH/41.1 mΩ
L_{RX}/R_{RX}	42.8 μH/70.2 mΩ
M	6.5 μH
L_{S1}/R_{S1}	20.8 μH/44.2 mΩ
C_{P1}/R_{CP1}	167.5 nF/9.3 mΩ
C_{S1}/R_{CS1}	192.8 nF/7.5 mΩ
L_{f1}/R_{Lf1} (n=3)	3.53 μH/9.2 mΩ
C_{f1}/R_{Cf1} (n=3)	1104 nF/44.2 mΩ
L_{f1}/R_{Lf1} (n=5)	0.92 μH/5.1 mΩ
C_{f1}/R_{Cf1} (n=5)	3956 nF/21.3 mΩ
L_{S2}/R_{S2}	7.1 μH/17.5 mΩ
C_{P2}/R_{CP2}	502.5 nF/6.7 mΩ
C_{S2}/R_{CS2}	100 nF/12.3 mΩ
L_{f2}/R_{Lf2} (n=3)	1.2 μH/6.3 mΩ
C_{f2}/R_{Cf2} (n=3)	3127 nF/4.6 mΩ
L_{f2}/R_{Lf2} (n=5)	0.33 μH/4.3 mΩ
C_{f2}/R_{Cf2} (n=5)	10062 nF/3.8 mΩ

shows the setup used to measure radiated noise from the TX and RX coils, and the loop antenna was 3 m away from the center of the TX and RX coils. Fig. 6 shows the EMI measurement results. To suppress the third or fifth harmonic magnetic field, L_{f1} and L_{f2} were set to $n = 3$ or 5 in Table I. As shown in Fig. 6(a), when n is 3, the proposed method can suppress the third harmonic magnetic field by 16.03 dB, compared to the conventional method. Also, as shown in Fig. 6(b), when n is 5, the proposed method can suppress the fifth harmonic magnetic field by 18.27 dB, compared to the conventional method. Table II shows the input and output voltage, current, output power, and dc–dc efficiency. The result indicates that the input voltage did not change, because the proposed method was designed so that it would not affect the operation of the WPT system. When L_f and C_f was added, the dc–dc efficiency decreased up to 0.6% due to parasitic resistance components. The fact that V_{DC} remains around 99 V implies the following. The added values of L_f and C_f satisfy (4), meaning that they do not affect the systems at the operating frequency. In other words, the proposed system has the advantage of maintaining the fundamental component, as described in (5), even with the addition of L_f and C_f, while selectively reducing only the harmonic components. This makes it a versatile technology with broad applicability.

TABLE II
VOLTAGE, CURRENT, AND EFFICIENCY RESULTS OF CONVENTIONAL AND PROPOSED METHODS

	Conventional	Proposed (n = 3)	Proposed (n = 5)
V_{DC} [V]	98.9	99.4	99.3
I_{DC} [A]	6.1	6.07	6.07
P_{DC} [W]	601	604	603
V_{OUT} [V]	90.9	90.9	91.3
I_{OUT} [A]	5.5	5.5	5.5
P_{OUT} [W]	501	500	502
DC–DC efficiency [%]	83.4	82.8	83.1

IV. CONCLUSION

This letter proposes a method for completely suppressing the harmonic magnetic field selectively. The double-sided *LCC* topology is modified to reduce the harmonic current of the TX and RX coils. The proposed method can selectively reduce the harmonic current flowing in the TX or RX coils to ideally zero, so the radiated noise can be suppressed to the maximum. The proposed method was verified through simulation and experiment. The experimental results showed that the proposed method can suppress EMI by 16.03 dB for the third harmonic and 18.27 dB for the fifth harmonic. As the power level of the WPT systems increases, this method will effectively suppress radiated noise to satisfy EMI regulation.

REFERENCES

[1] J. Ahn et al., "An out-of-phase wireless power transfer system for implantable medical devices to reduce human exposure to electromagnetic field and increase power transfer efficiency," *IEEE Trans. Biomed. Circuits Syst.*, vol. 16, no. 6, pp. 1166–1180, Dec. 2022.
[2] A. Sagar et al., "A comprehensive review of the recent development of wireless power transfer technologies for electric vehicle charging systems," *IEEE Access*, vol. 11, pp. 83703–83751, 2023.
[3] A. M. Jawad, H. M. Jawad, R. Nordin, S. K. Gharghan, N. F. Abdullah, and M. J. Abu-Alshaeer, "Wireless power transfer with magnetic resonator coupling and sleep/active strategy for a drone charging station in smart agriculture," *IEEE Access*, vol. 7, pp. 139839–139851, 2019.
[4] J. Park et al., "Planar multiresonance reactive shield for reducing electromagnetic interference in portable wireless power charging application," *Appl. Phys. Lett.*, vol. 114, no. 20, 2019, Art. no. 203902.
[5] S. Hong et al., "A frequency-selective EMI reduction method for tightly coupled wireless power transfer systems using resonant frequency control of a shielding coil in smartphone application," *IEEE Trans. Electromagn. Compat.*, vol. 61, no. 6, pp. 2031–2039, Dec. 2019.
[6] B. Sim et al., "A near field analytical model for EMI reduction and efficiency enhancement using an nth harmonic frequency shielding coil in a loosely coupled automotive WPT system," *IEEE Trans. Electromagn. Compat.*, vol. 63, no. 3, pp. 935–946, Jun. 2021.
[7] Y. Shin et al., "A LCL-LCL topology for odd harmonic magnetic fields reduction in over-coupled WPT system," in *Proc. Int. Symp. Electromagn. Compat.*, 2020, pp. 1–5.
[8] D. Kobuchi, K. Matsuura, Y. Narusue, and H. Morikawa, "Cancellation of harmonics in the magnetic field leakage from inductive power transfer systems," *IEEE Trans. Veh. Technol.*, vol. 72, no. 4, pp. 4442–4452, Apr. 2023.
[9] W. Li, H. Zhao, J. Deng, S. Li, and C. C. Mi, "Comparison study on SS and double-sided LCC compensation topologies for EV/PHEV wireless chargers," *IEEE Trans. Veh. Technol.*, vol. 65, no. 6, pp. 4429–4439, Jun. 2016.